JACS
JOURNAL OF THE AMERICAN CHEMICAL SOCIETY
pubs.acs.org/JACS
Article

# Hydroxide and Hydronium Ions Modulate the Dynamic Evolution of Nitrogen Nanobubbles in Water

Pengchao Zhang, Changsheng Chen, Muye Feng, Chao Sun,* and Xuefei Xu*

Cite This: J. Am. Chem. Soc. 2024, 146, 19537−19546
Read Online
ACCESS | Metrics & More | Article Recommendations | Supporting Information

**ABSTRACT:** It has been widely recognized that the pH environment influences the nanobubble dynamics and hydroxide ions adsorbed on the surface may be responsible for the long-term survival of the nanobubbles. However, understanding the distribution of hydronium and hydroxide ions in the vicinity of a bulk nanobubble surface at a microscopic scale and the consequent impact of these ions on the nanobubble behavior remains a challenging endeavor. In this study, we carried out deep potential molecular dynamics simulations to explore the behavior of a nitrogen nanobubble under neutral, acidic, and alkaline conditions and the inherent mechanism, and we also conducted a theoretical thermodynamic and dynamic analysis to address constraints related to simulation duration. Our simulations and theoretical analyses demonstrate a trend of nanobubble dissolution similar to that observed experimentally, emphasizing the limited dissolution of bulk nanobubbles in alkaline conditions, where hydroxide ions tend to reside slightly farther from the nanobubble surface than hydronium ions, forming more stable hydrogen bond networks that shield the nanobubble from dissolution. In acidic conditions, the hydronium ions preferentially accumulating at the nanobubble surface in an orderly manner drive nanobubble dissolution to increase the entropy of the system, and the dissolved nitrogen molecules further strengthen the hydrogen bond networks of systems by providing a hydrophobic environment for hydronium ions, suggesting both entropy and enthalpy effects contribute to the instability of nanobubbles under acidic conditions. These results offer fresh insights into the double-layer distribution of hydroxide and hydronium near the nitrogen−water interface that influences the dynamic behavior of bulk nanobubbles.

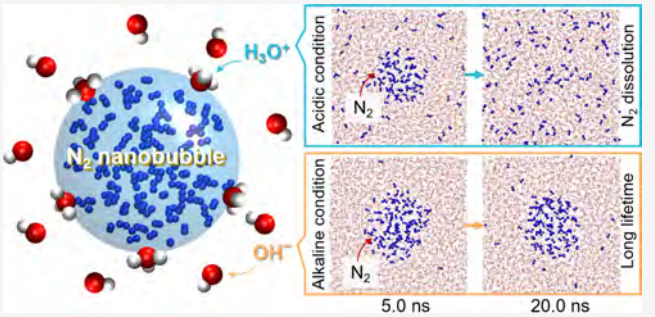




## 1. INTRODUCTION

Nanobubbles, characterized by their nanoscopic diameter, can be observed either adsorbed on submersed substrates, referred to as surface nanobubbles, or suspended in solutions, known as bulk nanobubbles.[1−4] Over the past two decades, nanobubbles have garnered considerable attention and found applications in diverse fields such as agriculture,[5] water treatment,[6,7] medicine,[8] mineral flotation,[9] cleaning,[10] food and beverage,[11] biochemistry,[12] enhanced reactions,[13] and lower cavitation threshold.[14]

The aforementioned applications are all founded on the premise of the existence of nanobubbles, signifying the long-term survival of the nanobubbles. In the case of surface nanobubbles, their stability can be effectively elucidated by the pinning-oversaturation mechanism.[15−19] When considering bulk nanobubbles, according to the classical Epstein−Plesset theory,[20] these nanobubbles should exhibit a brief lifetime, typically in the order of milliseconds. This contradicts the observed prolonged lifetimes in various studies.[7,21−26] The abnormal dynamic behavior of bulk nanobubbles remains a subject of ongoing debate. Experimental technologies such as dynamic light scattering and nanoparticle tracking analysis[25,27] face challenges in distinguishing between nanobubbles and variations in liquid density. Recent studies have raised suspicions regarding the existence of bulk nanobubbles, suggesting that the observed bulk nanoentities in experiments could potentially be nanodroplets, contaminant micelles, or nanoparticles, rather than true bulk nanobubbles.[28−30]

Considering that the existence of these bulk nanoentities, as evidenced, is closely tied to the saturation of dissolved gas,[31,32] we have rationale to speculate that at least a portion of these nanoentities observed in experiments are gas-filled and can be designated as nanobubbles. By presuming their presence under the initial conditions, in this work, we aim to investigate the dissolution dynamics of nanobubbles, evaluate their long-term survival, and reveal the mechanism by molecular simulations and theoretical analyses. This endeavor will contribute to a comprehensive understanding of fundamental scientific in-

Received: May 15, 2024
Revised: June 13, 2024
Accepted: June 14, 2024
Published: July 1, 2024




https://doi.org/10.1021/jacs.4c06641
J. Am. Chem. Soc. 2024, 146, 19537−19546

Table 1. Details of the Simulation Systems

| system | box size (Å$^3$) | no. of $H_2O$ | no. (molarity) of $H_3O^+$ | no. (molarity) of $OH^-$ | no. of $N_2$ |
|---|---|---|---|---|---|
| A | 55.0 × 55.0 × 55.0 | 5094 | 0 | 0 | 120 |
| B | 55.0 × 55.0 × 55.0 | 5074 | 20 (0.2 M) | 0 | 120 |
| C | 55.0 × 55.0 × 55.0 | 5074 | 0 | 20 (0.2 M) | 120 |
| D | 55.0 × 55.0 × 55.0 | 4994 | 0 | 100 (1.1 M) | 120 |

quiries about bubble dynamics, encompassing nucleation, growth, coalescence, and dissolution.[33−36] Ultimately, they are expected to contribute to numerous potential applications.

As known, multiple theories have been proposed in an attempt to elucidate the abnormal dynamic stability of bulk nanobubbles, including the skin model,[37,38] dynamic equilibrium model,[39] surfactant adsorption model,[40−42] surface charge model,[7,43−48] etc. Among these, the surface charge effect of bulk nanobubbles has garnered significant attention and discussion. Since negative zeta potentials for bulk nanobubbles in pure water, typically ranging from −50 mV to −20 mV, were observed,[4,7,49−51] it is often assumed that the surface charge of the bulk nanobubbles originates from surface-absorbed $OH^-$ ions, the only negatively charged species present in pure water. Furthermore, it has been noted that the nanobubble is more stable under alkaline conditions compared to acidic environments,[7,52,53] and the nanobubble surface exhibits a more negative zeta potential as pH rises.[54,55] Therefore, the adsorption of water self-ions ($OH^-$ and $H_3O^+$) at the nanobubble surface is thought to be a contributing factor to modulating the dynamics of bulk nanobubbles. However, the distribution propensity of $OH^-$ and $H_3O^+$ ions toward the bulk nanobubble surface and its impact on the dynamic stability of nanobubbles have not been conclusively understood. Further investigation is highly desired via atomic-level simulations, in particular, molecular dynamics (MD) simulations, to reveal a microscopic mechanism that elucidates the behavior of bulk nanobubbles in alkaline, acidic, or neutral environments.

To date, simulation research on bubble dynamics in water has predominantly employed classical all-atom MD[25,56−62] and coarse-grained MD.[57,60,61] These simulations have provided valuable insights into microscopic processes such as nucleation,[25] collision,[59] and dissolution[56−58,60−62] of bubbles. However, there is a lack of MD simulations that explicitly consider the presence of $OH^-$ and $H_3O^+$ ions in mimicking alkaline and acidic environments, respectively. The main challenge lies in accurately capturing the diffusion of $OH^-$ and $H_3O^+$ in water using nonreactive force fields because proton hopping plays a crucial role in ionic diffusion.[63,64] The proton hopping in water is a reactive process via the Grotthuss mechanism,[65−67] involving the formation and breakage of oxygen−hydrogen bonds. Describing this process requires using *ab initio* MD methods, which are resource-intensive and constrained for nanoscale spatial and temporal resolutions.

In the present work, we conducted deep potential molecular dynamics (DPMD) simulations[68,69] to investigate the behavior of nitrogen ($N_2$) nanobubbles in bulk water under neutral, alkaline, and acidic conditions. This approach combines the advantages of classical MD (efficiency) and *ab initio* MD (accuracy) methods by using deep potential (DP) trained by a neural network. Our findings qualitatively align with experimental results that the diffusion of $N_2$ molecules is slowed under alkaline conditions compared to pure water and acidic conditions. We reveal that the dynamic stability of $N_2$ nanobubbles is increased in alkaline environments due to a stable hydrogen bond (HB) network surrounding $OH^-$ ions, which are accumulated near the nanobubble surface.

Recent investigations on oil droplets have explained the negative charge and stability of bare oil droplets in water with the charge transfer from water to oil via interfacial C−H···O hydrogen bonds,[70,71] and the observation that nanobubbles are more (less) stable under alkaline (acidic) conditions mirrors the behavior of hydrophobic oily nano-objects in water, further enriching the parallelism and broadening the scope of the present study.

## 2. COMPUTATIONAL DETAILS

**2.1. Deep Potential Model.** In this work, the data sets for training the deep potential model were generated by a concurrent learning scheme with DP Generator (DP-GEN),[72] which involves three iterative steps: DP training in DeePMD-kit,[68,69] DPMD exploration in LAMMPS,[73] and density functional theory (DFT) labeling in VASP.[74,75]

In the DFT labeling stage, the exchange−correlation interaction was treated by using a meta-generalized-gradient-approximation (meta-GGA) known as the strongly constrained and appropriately normed (SCAN) semilocal density functional,[76] which has been demonstrated to be able to well describe the electrical, structural, and dynamic properties of water molecules and water self-ions in previous tests.[63,77−82] A plane wave basis set with a cutoff energy of 600 eV was employed. The Brillouin zone was sampled by using a single k-point. Gaussian smearing with a width of 0.05 eV was used for partial orbital occupancies.[83] The electronic self-consistent loop was terminated when the global break condition reached $1 \times 10^{-5}$ eV.

During the DP-GEN iterations, the conformational space was sampled extensively by performing explorations with various combinations of thermodynamic parameters, including canonical ensemble and isothermal−isobaric ensemble, temperatures ranging from 270 to 600 K, and pressures from 0.2 to 900 bar. Finally, a total of 16 subsystem data sets, incorporating $H_2O$, $H_3O^+$, $OH^-$, and $N_2$, have been collected and segmented into the training and test data sets (refer to Table S1). The final DP model was trained based on the training data set containing 91,179 configurations and validated by the independent test data set containing 8978 configurations with energies and forces calculated by SCAN. The DP model has root-mean-square errors (RMSEs) of 0.91 meV/atom for energy and 39 meV/Å for atomic force as compared to the SCAN reference values, demonstrating its satisfactory precision. For additional details regarding the DP-GEN iteration and DP model training, please refer to Supporting Information.

**2.2. DPMD Simulations.** DPMD simulations were conducted using the LAMMPS software[73] to evaluate the dynamic behavior of $N_2$ nanobubbles in neutral, acidic, and alkaline environments. In the neutral system (labeled as system A in Table 1), an initial nanobubble comprising 120 $N_2$


https://doi.org/10.1021/jacs.4c06641
J. Am. Chem. Soc. 2024, 146, 19537−19546

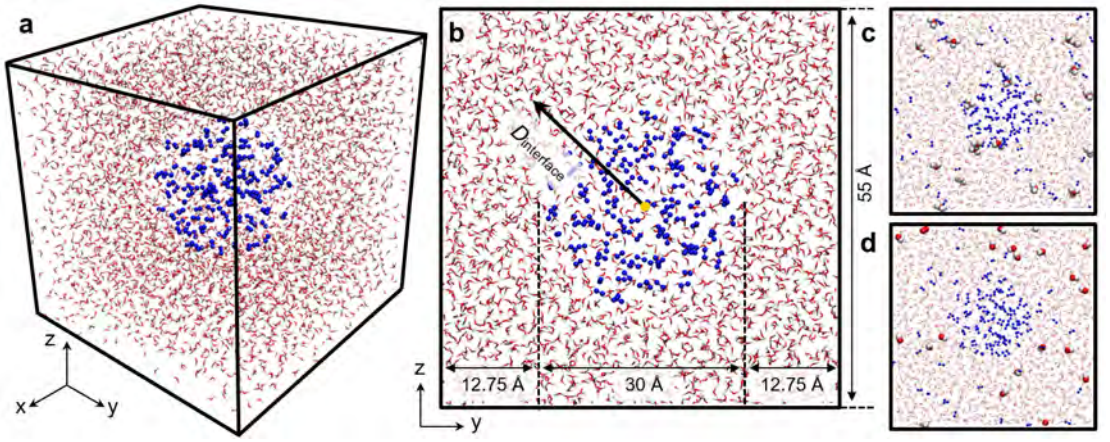


**Figure 1.** Schematic diagrams of bulk nitrogen nanobubbles. (a) Three-dimensional and (b) central cross-sectional views of system A (see Table 1), depicting the $N_2$ nanobubble positioned at the center of a periodic cubic box filled with pure water. (c) Snapshot of system B, showing the $N_2$ nanobubble immersed in water containing 20 $H_3O^+$ ions. (d) Snapshot of system C, illustrating the $N_2$ nanobubble surrounded by water and 20 $OH^-$ ions. The $H_3O^+$, $OH^-$, and $N_2$ species are represented by using a ball model, while the $H_2O$ molecules are depicted by using a stick model. Color code: hydrogen, white; nitrogen, blue; oxygen, red.

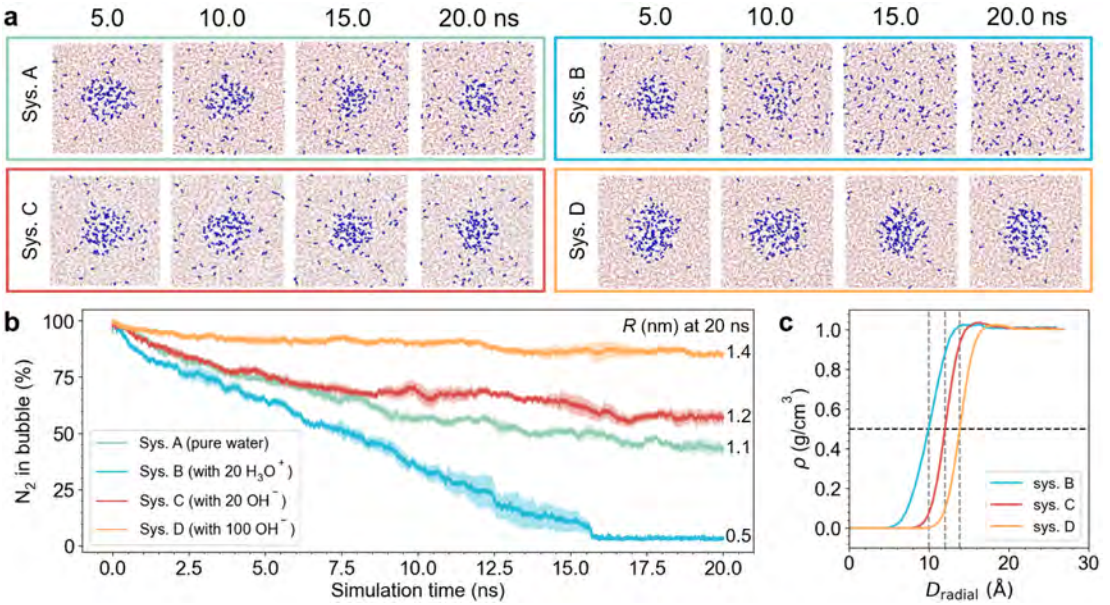


**Figure 2.** The dynamic evolution of nitrogen nanobubble in different systems. (a) Snapshots during 5−20 ns simulations for four systems, namely, A (pure water without self-ions), B (water with 20 $H_3O^+$), C (water with 20 $OH^-$), and D (water with 100 $OH^-$). (b) Time-evolution of the percentage of $N_2$ molecules in the nanobubble during 0−20 ns, with transparent colors indicating the standard deviations from four independent simulations. (c) Average water density along the radial distance from the nanobubble center during 5−12.5 ns.

molecules with a diameter of 3 nm was positioned within a periodic cube box containing around 5000 $H_2O$ molecules, with a side length of 5.5 nm (Figure 1a,b). In the acidic system (labeled as system B) and the alkaline system (labeled as system C), 20 $H_3O^+$ and 20 $OH^-$ ions are introduced into the bulk water, respectively, as illustrated in Figure 1c,d, corresponding to pH values of 0.66 and 13.34, respectively. Furthermore, in order to enhance the effect of $OH^-$ during the limited simulation time, 100 $OH^-$ ions were incorporated into the water bulk (referred to as system D in Table 1) to emulate a more alkaline environment.

All simulations were performed in the isothermal−isobaric ensemble (*NPT*) at a temperature of 330 K and a pressure of 1 atm. Here, we used a 30 K higher temperature in simulations than the target ambient conditions because it had been shown that a temperature increase of 30−40 K in the SCAN-based classical simulations can better simulate various properties of liquid water,[84−86] possibly by mitigating the overstructuring of intermolecular interactions.[87] This treatment helped align the diffusion coefficients of $OH^-$, $H_3O^+$, and $H_2O$ with their experimental values at ambient conditions.[63,80,82] Temperature and pressure were maintained using the Nosé−Hoover thermostat and barostat[88,89] with damping times of 0.1 and 1 ps, respectively. We ran four independent trajectories for each system, with each trajectory spanning 20 ns and a time step of 1 fs. Data analysis was performed at intervals of 1 ps.

## 3. RESULTS AND DISCUSSION

**3.1. Evolution of Nitrogen Nanobubbles.** First, the time evolution of the number of $N_2$ molecules in the bulk



https://doi.org/10.1021/jacs.4c06641
J. Am. Chem. Soc. 2024, 146, 19537−19546

nanobubble was monitored during the 20 ns simulation. As depicted in Figure 2a,b, the nanobubble lifetime is significantly shorter under acidic conditions (system B) compared to the neutral and alkaline conditions, with all $N_2$ molecules dissolving into the water bulk after ∼16 ns. In contrast, in systems A, C, and D, 42%, 54%, and 84% of $N_2$ molecules (corresponding to the nanobubble radii of 1.1, 1.2, and 1.4 nm, respectively) remain in the nanobubble after 20 ns. It indicates that alkaline conditions stabilize the bulk nanobubble, and increasing the number of $OH^-$ ions from 20 to 100 remarkably extends its lifetime. This trend aligns with previous experimental observations that a higher number of nanobubbles are detected under alkaline conditions.[7,48,52,53]

For 5−12.5 ns of simulations, during which the bulk nanobubble persists without complete dissolution, in all cases, we plotted the average water density along the radial distance from the nanobubble center to the water bulk in Figure 2c. The position where the water mass density is half that of the bulk water is usually approximately defined as the Gibbs dividing surface (GDS) separating the water phase and gas phase.[63,90,91] Based on this definition of GDS, we estimate the averaged radius of the nanobubble during the 5−12.5 ns simulations to be 10, 12, and 14 Å in systems B, C, and D, respectively (Figure 2c), and we designate the region near the GDS as the nitrogen−water interface in the following analysis.

**3.2. Ionic Double-Layer Distribution in the Interface and its Impact on the Nanobubble Stability.** We now shift our focus to the microscopic effects of the ions. The spatial distribution analysis of $H_3O^+$ and $OH^-$ ions surrounding the $N_2$ nanobubble is illustrated in Figure 3a, which shows that the $H_3O^+$ and $OH^-$ ions prefer to enrich near the nitrogen-water interface, but in separate layers. A similar phenomenon has been observed and referred to as the interfacial double-layer distribution of self-ions in our recent work for the flat air−water interface.[63,92] In the nitrogen−water interface of the current bulk nanobubble system, $H_3O^+$ ions predominantly occupy the top layer of the water phase, with a high peak of distribution at ∼ −1 Å relative to the GDS; in contrast to the observation in the flat air−water interface,[63,92] $OH^-$ ions show a weak interfacial propensity as compared to $H_3O^+$, nevertheless, the maximum of volume normalized number distribution of $OH^-$ along the normal distance to the nanobubble surface appears in a deeper interfacial layer on the water side, corresponding to a depth of 2−4 water-molecule layers (∼−5 Å) below the GDS. The thickness of such an ionic double-layer is approximately 4 Å based on the current simulations.

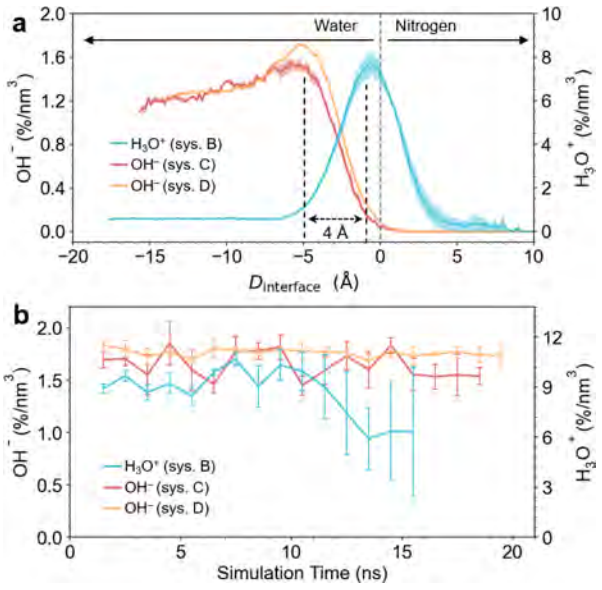


**Figure 3.** The distribution of hydronium and hydroxide ions. (a) Volume normalized number distribution of water self-ions along the normal distance to the nitrogen−water interface during 5−12.5 ns. The normal distance is defined as negative on the water side, zero at the GDS, and positive on the nanobubble side. (b) Maximum value change tendency of volume normalized number distribution of water self-ions.

Figure 3b shows that the concentration distribution of $OH^-$ ions at the nitrogen−water interface exhibits a notable degree of stability over 20 ns. Although the peak concentration of $H_3O^+$ ions is remarkably higher than that of $OH^-$ ions, it gradually diminishes with the shrinking of the nanobubble after ∼10 ns. Furthermore, the $OH^-$ ions exhibit a more delocalized distribution throughout the interface region (within the range of −15 to −4 Å), compared to the narrow distribution of $H_3O^+$ ions. Therefore, it is plausible that in the pure water system, the positive charge associated with $H_3O^+$ ions is partly offset or screened by the neighboring $OH^-$ layer characterized by a more pronounced negative charge. Besides, the outer $OH^-$ layer of the nanobubble may be more possibly correspond to the experimental detection region,[63] also lending support to the macroscopic measurements of negative zeta potential of bulk nanobubble typically falling within the range of −50 mV to −20 mV.[4,7,49−51]

The formation of this ionic double-layer near the bulk nanobubble surface is due to the different amphipathies of $H_3O^+$ and $OH^-$ ions. As revealed in Figure 4a, the dipole vectors of $H_3O^+$ ions are predominantly aligned parallel to the interfacial normal vector with cos $\theta$ = ∼1.0, where $\theta$ is the angle between the normal vector of the interface and the dipole vector of the self-ions. The orientation distribution can be attributed to the preference of $H_3O^+$ ions to lie flat on the uppermost water surface with their hydrophobic oxygen atom facing the $N_2$ nanobubble and their hydrophilic protons neighboring $H_2O$ molecules.[64,93,94] In contrast, the orientation of $OH^-$ is more random (cos $\theta$ = −1.0 to 1.0) because its oxygen atom with more delocalized lone pair electrons is a much better HB acceptor than both oxygens of $H_3O^+$ and water molecule, and thus, $OH^-$ ions can stay in a deeper water layer of the interface to form abundant HB network with surrounding water molecules.[63]

The distribution of water self-ions near the bulk nanobubble surface and the corresponding HB network character determine the nanobubble dynamics. Under the acidic conditions, first, due to the orderly arrangement of $H_3O^+$ ions surrounding the nanobubble, the system has a low entropy, driving the nanobubble dissolution. Second, since the $H_3O^+$ ions prefer to occupy the inner layer of the nitrogen−water interface (at ∼−1 Å relative to the GDS), the hydrophobic nature of dissolved $N_2$ will make them preferentially pass through $H_3O^+$, which also provides a more hydrophobic environment for $H_3O^+$ ions, consequently strengthening their and neighboring water's HB networks. It is evidenced by a very slight rise in the HB number of each $H_3O^+$ from ∼3.04 to ∼3.10 and a significant increase in the HB number of each neighboring $H_2O$ from ∼3.47 to ∼3.64 within 20 ns (system B in Figure 4b). This lowers the enthalpy of the


https://doi.org/10.1021/jacs.4c06641
J. Am. Chem. Soc. 2024, 146, 19537−19546

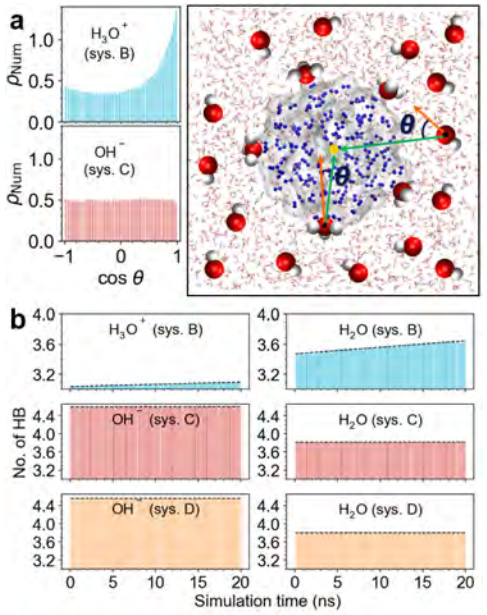


**Figure 4.** Orientation and HB network of water self-ions. (a) Orientation distributions of $OH^-$ and $H_3O^+$ during 5−12.5 ns. Hist bars represent the cumulative number density, $\rho_{Num}$ of self-ions within statistical intervals. The orientation of the ions is determined by the cosine of the $\theta$ angle, which is the angle between the normal vector (from the nitrogen−water interface to the nanobubble center, depicted by green arrows) of the interface and the dipole vector (from the hydrogen center to oxygen, depicted by orange arrows) of the self-ions. (b) Evolution of HB numbers for each $OH^-$, $H_3O^+$, and neighboring $H_2O$ (i.e., $H_2O$ in the first shell of water self-ions) during 0−20 ns, where black dashed lines represent the linear fitting.

system and further promotes $N_2$ diffusion from the nanobubble into the water. Thereby, entropy and enthalpy effects contribute together to the instability of nanobubbles under acidic conditions. In alkaline conditions, the excess $OH^-$ ions randomly enriching at a deeper interface layer on the water side establish a stable enough HB network by the hyper-coordinated solvation, just as what we notice for systems C and D in Figure 4b, and the HB number of $OH^-$ remains almost unchanged during the 20 ns simulation. It implies that the stable HB network of surrounding $OH^-$ ions may slow down the dissolution of $N_2$ nanobubble. In the neutral condition, the impacts of $H_3O^+$ and $OH^-$ ions separately distributed in the different interface layers may compete with each other, rendering a compromised nanobubble stability as compared to that under the alkaline condition.

In summary, the dynamic behavior of the $N_2$ nanobubble is found to be closely correlated with the interfacial distribution and orientation of $H_3O^+$ and $OH^-$ ions and their surrounding solvation environment. These microscopic-level details provide new insights into the stability of bulk nanobubbles. However, it is also important to acknowledge that bulk nanobubbles exhibit limited dynamic behavior during a brief 20 ns simulation time. To overcome this limitation, we next utilize theoretical models, incorporating simulation data from neutral and alkaline systems and experimental parameters, to further explore and analyze the thermodynamic and dynamic behaviors of bulk nanobubbles.

**3.3. Theoretical Thermodynamic and Dynamic Analysis.** The classical nucleation theory can describe the evolution of small gas nanobubbles from a thermodynamic aspect. In particular, for the charged gas nanobubble in the *NPT* ensemble, changes of Gibbs free energy ($dG$) with the radius of $R$ (related to the volume of the nanobubble ($V_2$) and the number of nitrogen molecules within the nanobubble ($N_{g,2}$)) can be expressed as

$$dG = \left(p_1 + \frac{2\gamma}{R} - p_2 - \frac{Q^2}{32\pi^2\epsilon R^4}\right)dV_2 + (\mu_{g,2} - \mu_{g,1})dN_{g,2} \quad (1)$$

where $p_1$ and $p_2$ represent the pressures of the liquid and gas phases, respectively. The $\gamma$ and $\epsilon$ denote, respectively, the surface tension and the dielectric constant of the medium. $Q$ is the nanobubble surface charge, and $\mu_{g,2}$ and $\mu_{g,1}$ are the chemical potentials of the nitrogen molecule in the gas phase and liquid phase, respectively (see the Supporting Information for more details).

When $dG = 0$, the thermodynamic equilibrium of the nanobubble is reached. According to eq 1, the thermodynamic equilibrium also means the equations $(\mu_{g,2} - \mu_{g,1})dN_{g,2} = 0$ and $\left(p_1 + \frac{2\gamma}{R} - p_2 - \frac{Q^2}{32\pi^2\epsilon R^4}\right)dV_2 = 0$, that is, they, respectively, satisfy the criterion for chemical equilibrium

$$\mu_{g,1} = \mu_{g,2} \quad (2)$$

and mechanical equilibrium[44,95−97]

$$p_1 + \frac{2\gamma}{R} = p_2 + \frac{Q^2}{32\pi^2\epsilon R^4} \quad (3)$$

where the right side of eq 3 represents the expansion force, and the left side represents the collapse force acting on the nanobubble. When the electrostatic term $\frac{Q^2}{32\pi^2\epsilon R^4}$ is omitted, eq 3 simplifies to the classical Young−Laplace equation.[9]

It is usually assumed that mechanical equilibrium (eq 3) is reached more quickly than chemical equilibrium (eq 2),[98] that is, the thermodynamic equilibrium is dominantly controlled by the chemical equilibrium. We then simplify eq 1 by using a detailed expansion of the chemical potentials

$$dG = k_B T \ln\left(\frac{p_2 H}{c_{g,1}}\right)dN_{g,2} \quad (4)$$

where $k_B$ is the Boltzmann constant, $T$ denotes the simulation temperature, $c_{g,1}$ represents the actual concentration of nitrogen in the liquid phase, and $H$ denotes the Henry coefficient of nitrogen gas. Next, by establishing a relationship between $p_2$ and $R$ by solving the mechanical equilibrium equation (eq 3) and the van der Waals equation,[99] the free energy change with the evolution of nanobubble (namely, $\frac{dG}{dN_{g,2}}$) can be determined. See the Supporting Information for the details.

The numerical solution of eq 4 is presented in Figure 5a, which shows that in the neutral condition (system A), the free energy decreases monotonically with the decrease of the number of $N_2$ molecules in the nanobubble. This observation suggests that the $N_2$ nanobubble prefers to completely dissolve into the water to approach a more stable state. In system C containing 20 $OH^-$ ions, the free energy decreases as the nanobubble dissolves until reaching a minimum when only two $N_2$ molecules are left, suggesting near-complete dissolution. In


https://doi.org/10.1021/jacs.4c06641
J. Am. Chem. Soc. 2024, 146, 19537−19546

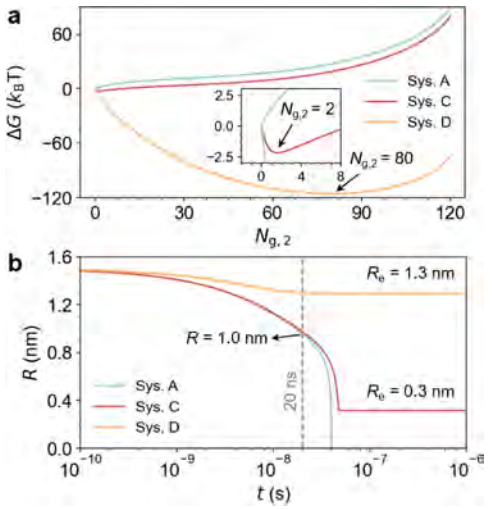


**Figure 5.** Theoretical thermodynamic and dynamic evolution of nitrogen nanobubble. (a) Evolution of the Gibbs free energy ($\Delta G$) with the number of $N_2$ molecules ($N_{g,2}$) within the bulk nanobubble. The $N_{g,2}$ corresponding to the minimum of free energy is marked for systems C and D. (b) Dynamic evolution of nanobubble radius $R$ in different systems, where the equilibrium radius $R_e$ is given for systems C and D.

system D with 100 $OH^-$ ions, the free energy gradually decreases, followed by an increase with decreasing number of $N_2$ molecules in the nanobubble. A distinct free energy minimum well of about −115 $k_BT$ is located when 80 $N_2$ molecules remain in the nanobubble. The corresponding equilibrium radius is around 1.3 nm.

We can further explore the nanobubble equilibrium from a dynamic aspect. For an individual spherical nanobubble, the dissolution dynamics can be estimated using the Epstein–Plesset equation[20]

$$\frac{dR}{dt} = \frac{D}{\rho}(c_{g,1} - Hp_2)\left(\frac{1}{R} + \frac{1}{\sqrt{\pi Dt}}\right) \quad (5)$$

where $t$ represents the evolution time, $\rho$ is the density of the gas inside the nanobubble, and $D$ is the diffusion coefficient of nitrogen gas (for more information, please refer to Supporting Information).

The analysis results are presented in Figure 5b. It is evident that in pure water (system A), the radius of the nanobubble exhibits a decreasing trend until ultimate extinction at ∼40 ns. In system C with 20 $OH^-$ ions, the decreasing nanobubble radius experiences a sudden cessation at ∼47 ns and stabilizes at 0.3 nm, and thus the equilibrium radius $R_e$ of nanobubble is estimated to be 0.3 nm, which corresponds to a nanobubble containing two $N_2$ molecules, in good agreement with our thermodynamic analysis result shown in Figure 5a. In addition, we also notice that the present theoretical analysis predicts a nanobubble radius of ∼1 nm at 20 ns for both systems A and C, which reasonably agree with our simulation outcomes. As illustrated in Figure 2b, the DPMD simulations show that in systems A and C, the nanobubble radii at 20 ns are approximately 1.1 and 1.2 nm, respectively.

In system D with 100 $OH^-$ ions, the simulation results exhibit closer alignment with the theoretical calculation. The nanobubble is stabilized at a radius of 1.3 nm (Figure 5b) over the microsecond time scale. This stability approximately aligns with the observation of the DPMD simulation, where the radius slowly approaches 1.4 nm at 20 ns (Figure 2b). Although there still is a slight decrease trend in radius in the end of the current 20 nm simulation, it is believed that the nanobubble will exhibit a lifetime in the microsecond range in a longer simulation. These findings further corroborate the thermodynamic prediction (Figure 5a).

**3.4. Discussion on Limitations and Applications.** The current model system describing a 3 nm nanobubble in water is much smaller than most nanobubbles in practical scenarios, which typically have a diameter of around 100 nm. Notably, Jadhav and Barigou[27] demonstrated the existence of the cluster of bulk nanobubbles in neutral or alkaline conditions, and under acidic conditions, these nanoentities dissociated into minuscule clusters of around 1 nm, which aligns with the size of our simulated nanobubbles. Our simulations also directly mimic a situation similar to the cluster of nanobubbles by extending the periodic box. In addition, although the disparity in curvature may result in large variations in some physical properties, for example, surface tension, which could have an important impact on the dynamic behavior of nanobubbles, the current 3 nm nanobubble simulation still can offer significant insights into nanobubbles with a larger size at the microscopic level.

In the pursuit of efficiency, another limitation of the current simulations is that we did not incorporate nuclear quantum effects (NQEs), which could be caught only by using Feynman path-integral formalisms.[100] This might be at the root of some quantitative discrepancies in the present simulations.

To ensure adequate sampling within a limited time frame and a smaller box size, we conducted separate simulations for the systems containing $OH^-$ and $H_3O^+$ ions to prevent ionic recombination into water molecules, thus ensuring the efficiency of the statistical analysis. Our primary focus is on studying the effects of $OH^-$ and $H_3O^+$ ions, rather than the influence of other ions on the main results. The current simulations overlook the effects of counterbalancing ions; nonetheless, previous studies have indicated that the DP model relies on local environmental features, suggesting that counterbalancing ions may not be necessary.[63]

Furthermore, the construction of the DP model in this work relies on the assumption of short-range interactions, and long-range electrostatic interactions are not explicitly accounted for. Since the magnitude of long-range electrostatic interactions is much lower than that of short-range many-body interactions, the current DP model can be perceived as a leading-order approximation of DFT interactions for effectively capturing the primary physical phenomena inherent in the system.

Considering the $N_2$ solubility in water and the number of water molecules in DPMD simulations (refer to Table 1), it becomes evident that the system is oversaturated if one $N_2$ molecule in the nanobubble diffuses into the solution. This ensures that all the examined systems are oversaturated at an early stage of the simulation, akin to observations in classical MD studies.[58] Furthermore, operating under such supersaturation of $N_2$ gas in the liquid phase, our theoretical analysis can align with the assumptions of achieving chemical and mechanical equilibrium under the *NPT* ensemble.

Despite the acknowledged limitations, we are confident that the current findings provide, at least, a qualitative comprehension of how the distribution of the ionic double-layer influences the dynamics of $N_2$ nanobubbles. This research may facilitate insights for future fundamental studies and a wide array of potential industrial applications. For instance, the pH


https://doi.org/10.1021/jacs.4c06641
J. Am. Chem. Soc. 2024, 146, 19537−19546

in a solution can exert an impact on the lifespan of nanobubbles, which could reduce the threshold for the occurrence of cavitation.[14,101,102] Furthermore, our findings regarding the distribution of $OH^-$ and $H_3O^+$ ions may be expected to influence various processes such as flotation, electrophoresis, and enhanced interfacial reactions.[103−108]

## 4. CONCLUSION

In summary, we trained a highly accurate and efficient neural network potential to conduct molecular dynamics simulations, aiming to investigate the dynamic behavior of nitrogen nanobubbles under neutral, acidic, and alkaline conditions at the microscopic level. Our DPMD simulation results, which are self-consistent with theoretical models, exhibit a qualitatively similar trend of bubble dissolution with experimental observations, highlighting the limited dissolution of bulk nanobubble in alkaline conditions compared to neutral and acidic environments.[7,48,52,53,53]

We ascertained the presence of the double-layer distribution of $OH^-$ and $H_3O^+$ ions near the nitrogen−water interface, which is aligned with our recent work on the air(oil)−water interface.[63,92] In the microscopic view of molecular structures, we reveal that the shielding effect of hypercoordinated solvation of $OH^-$ ions limits the diffusive outflow of $N_2$ molecules, while $H_3O^+$ ions enriched closely at the nanobubble surface in an orderly orientation induce the dissolution of $N_2$ nanobubbles to stabilize the system by increasing the entropy of the system and strengthening of the hydrogen bond network.

The present study, which combines deep potential molecular dynamics simulations with theoretical analysis, offers valuable insights into the effects of pH on bubble dynamics with significant implications in the fields of chemistry, biology, and engineering. Looking ahead, we anticipate that future advancements in analytical techniques, such as surface-sensitive vibrational spectroscopies,[109,110] capable of probing different layers of the nitrogen−water interface, may provide detailed information on surface properties. We believe that integrating these techniques with our results will result in a more comprehensive understanding of the surface properties of the gas−liquid interface.

## ■ ASSOCIATED CONTENT

### Data Availability Statement

The simulation and visualization software packages used to do the calculations are freely available. The requisite input files for replicating the research can be accessed at https://github.com/Zhang-pchao/N2BubbleIon.

### Supporting Information

The Supporting Information is available free of charge at https://pubs.acs.org/doi/10.1021/jacs.4c06641.

Building data sets, DFT calculation, and DP model training, thermodynamic analysis of nanobubble stability and dynamic analysis of nanobubble dissolution, as well as other discussions and details (PDF)

Videos demonstrating the dynamic behavior of nitrogen nanobubbles under neutral, acidic, and alkaline conditions (ZIP)

## ■ AUTHOR INFORMATION


### Corresponding Authors

**Chao Sun** − *Center for Combustion Energy, Department of Energy and Power Engineering, and Key Laboratory for Thermal Science and Power Engineering of Ministry of Education, New Cornerstone Science Laboratory, and Department of Engineering Mechanics, School of Aerospace Engineering, Tsinghua University, Beijing 100084, China;* orcid.org/0000-0002-0930-6343; Email: chaosun@tsinghua.edu.cn

**Xuefei Xu** − *Center for Combustion Energy, Department of Energy and Power Engineering, and Key Laboratory for Thermal Science and Power Engineering of Ministry of Education, Tsinghua University, Beijing 100084, China;* orcid.org/0000-0002-2009-0483; Email: xuxuefei@tsinghua.edu.cn

### Authors

**Pengchao Zhang** − *Center for Combustion Energy, Department of Energy and Power Engineering, and Key Laboratory for Thermal Science and Power Engineering of Ministry of Education, Tsinghua University, Beijing 100084, China;* orcid.org/0000-0002-6556-6588

**Changsheng Chen** − *Center for Combustion Energy, Department of Energy and Power Engineering, and Key Laboratory for Thermal Science and Power Engineering of Ministry of Education, Tsinghua University, Beijing 100084, China;* orcid.org/0000-0003-2836-9160

**Muye Feng** − *School of Mechanical and Power Engineering, Nanjing Tech University, Nanjing 211816, China;* orcid.org/0000-0003-4050-8901

Complete contact information is available at: https://pubs.acs.org/10.1021/jacs.4c06641


### Notes

The authors declare no competing financial interest.

## ■ ACKNOWLEDGMENTS

This work was partially supported by the National Natural Science Foundation of China (Grant Nos. 11988102, 21973053, and 52106164). The authors would like to acknowledge the valuable discussions with Professor Mingbo Li and Xiaotong Ma. Computational resources were partially provided by the High Performance Computing (HPC) platform at Tsinghua University.

## ■ REFERENCES


(1) Seddon, J. R.; Lohse, D. Nanobubbles and Micropancakes: Gaseous Domains on Immersed Substrates. *J. Phys.: Condens. Matter* **2011**, *23*, 133001.

(2) Alheshibri, M.; Qian, J.; Jehannin, M.; Craig, V. S. A History of Nanobubbles. *Langmuir* **2016**, *32*, 11086−11100.

(3) Tan, B. H.; An, H.; Ohl, C.-D. Stability of Surface and Bulk Nanobubbles. *Curr. Opin. Colloid Interface Sci.* **2021**, *53*, 101428.

(4) Zhou, L.; Wang, S.; Zhang, L.; Hu, J. Generation and Stability of Bulk Nanobubbles: A Review and Perspective. *Curr. Opin. Colloid Interface Sci.* **2021**, *53*, 101439.

(5) Ebina, K.; Shi, K.; Hirao, M.; Hashimoto, J.; Kawato, Y.; Kaneshiro, S.; Morimoto, T.; Koizumi, K.; Yoshikawa, H. Oxygen and Air Nanobubble Water Solution Promote the Growth of Plants, Fishes, and Mice. *PLoS One* **2013**, *8*, No. e65339.

(6) Zhang, Y.; Han, Y.; Ji, X.; Zang, D.; Qiao, L.; Sheng, Z.; Wang, C.; Wang, S.; Wang, M.; Hou, Y.; Chen, X.; Hou, X. Continuous Air

Purification by Aqueous Interface Filtration and Absorption. *Nature* **2022**, *610*, 74−80.
(7) Nirmalkar, N.; Pacek, A.; Barigou, M. On the Existence and Stability of Bulk Nanobubbles. *Langmuir* **2018**, *34*, 10964−10973.
(8) Lukianova-Hleb, E. Y.; Campbell, K. M.; Constantinou, P. E.; Braam, J.; Olson, J. S.; Ware, R. E.; Sullivan, D. J.; Lapotko, D. O. Hemozoin-Generated Vapor Nanobubbles for Transdermal Reagent- and Needle-Free Detection of Malaria. *Proc. Natl. Acad. Sci. U. S. A.* **2014**, *111*, 900−905.
(9) Tao, D. Recent Advances in Fundamentals and Applications of Nanobubble Enhanced Froth Flotation: A Review. *Miner. Eng.* **2022**, *183*, 107554.
(10) Zhu, J.; An, H.; Alheshibri, M.; Liu, L.; Terpstra, P. M.; Liu, G.; Craig, V. S. Cleaning With Bulk Nanobubbles. *Langmuir* **2016**, *32*, 11203−11211.
(11) Safonov, V. L.; Khitrin, A. K. Hydrogen Nanobubbles in a Water Solution of Dietary Supplement. *Colloids Surf., A* **2013**, *436*, 333−336.
(12) Wang, Y.; Shen, Z.; Guo, Z.; Hu, J.; Zhang, Y. Effects of Nanobubbles on Peptide Self-Assembly. *Nanoscale* **2018**, *10*, 20007−20012.
(13) Wang, L.; Ali, J.; Wang, Z.; Oladoja, N.; Cheng, R.; Zhang, C.; Mailhot, G.; Pan, G. Oxygen Nanobubbles Enhanced Photodegradation of Oxytetracycline Under Visible Light: Synergistic Effect and Mechanism. *Chem. Eng. J.* **2020**, *388*, 124227.
(14) Gao, Z.; Wu, W.; Wang, B. The Effects of Nanoscale Nuclei on Cavitation. *J. Fluid Mech.* **2021**, *911*, A20.
(15) Liu, Y.; Zhang, X. Nanobubble Stability Induced by Contact Line Pinning. *J. Chem. Phys.* **2013**, *138*, 014706.
(16) Weijs, J. H.; Lohse, D. Why Surface Nanobubbles Live for Hours. *Phys. Rev. Lett.* **2013**, *110*, 054501.
(17) Liu, Y.; Wang, J.; Zhang, X.; Wang, W. Contact Line Pinning and the Relationship between Nanobubbles and Substrates. *J. Chem. Phys.* **2014**, *140*, 054705.
(18) Tan, B. H.; An, H.; Ohl, C.-D. Resolving the Pinning Force of Nanobubbles With Optical Microscopy. *Phys. Rev. Lett.* **2017**, *118*, 054501.
(19) Theodorakis, P. E.; Che, Z. Surface Nanobubbles: Theory, Simulation, and Experiment. A Review. *Adv. Colloid Interface Sci.* **2019**, *272*, 101995.
(20) Epstein, P. S.; Plesset, M. S. On the Stability of Gas Bubbles in Liquid-Gas Solutions. *J. Chem. Phys.* **1950**, *18*, 1505−1509.
(21) Liu, Y.; Zhang, X. A Unified Mechanism for the Stability of Surface Nanobubbles: Contact Line Pinning and Supersaturation. *J. Chem. Phys.* **2014**, *141*, 134702.
(22) Chan, C. U.; Chen, L.; Arora, M.; Ohl, C.-D. Collapse of Surface Nanobubbles. *Phys. Rev. Lett.* **2015**, *114*, 114505.
(23) Azevedo, A.; Etchepare, R.; Calgaroto, S.; Rubio, J. Aqueous Dispersions of Nanobubbles: Generation, Properties and Features. *Miner. Eng.* **2016**, *94*, 29−37.
(24) Ohgaki, K.; Khanh, N. Q.; Joden, Y.; Tsuji, A.; Nakagawa, T. Physicochemical Approach to Nanobubble Solutions. *Chem. Eng. Sci.* **2010**, *65*, 1296−1300.
(25) Weijs, J. H.; Seddon, J. R.; Lohse, D. Diffusive Shielding Stabilizes Bulk Nanobubble Clusters. *ChemPhysChem* **2012**, *13*, 2197−2204.
(26) Ghaani, M. R.; Kusalik, P. G.; English, N. J. Massive Generation of Metastable Bulk Nanobubbles in Water by External Electric Fields. *Sci. Adv.* **2020**, *6*, No. eaaz0094.
(27) Jadhav, A. J.; Barigou, M. On the Clustering of Bulk Nanobubbles and Their Colloidal Stability. *J. Colloid Interface Sci.* **2021**, *601*, 816−824.
(28) Alheshibri, M.; Jehannin, M.; Coleman, V. A.; Craig, V. S. Does Gas Supersaturation by a Chemical Reaction Produce Bulk Nanobubbles? *J. Colloid Interface Sci.* **2019**, *554*, 388−395.
(29) Jadhav, A. J.; Barigou, M. Bulk Nanobubbles or Not Nanobubbles: That Is the Question. *Langmuir* **2020**, *36*, 1699−1708.
(30) Jaramillo-Granada, A. M.; Reyes-Figueroa, A.; Ruiz-Suárez, J. Xenon and Krypton Dissolved in Water Form Nanoblobs: No Evidence for Nanobubbles. *Phys. Rev. Lett.* **2022**, *129*, 094501.
(31) Qiu, J.; Zou, Z.; Wang, S.; Wang, X.; Wang, L.; Dong, Y.; Zhao, H.; Zhang, L.; Hu, J. Formation and Stability of Bulk Nanobubbles Generated by Ethanol−Water Exchange. *ChemPhysChem* **2017**, *18*, 1345−1350.
(32) Eklund, F.; Swenson, J. Stable Air Nanobubbles in Water: The Importance of Organic Contaminants. *Langmuir* **2018**, *34*, 11003−11009.
(33) Prakash, R.; Lee, J.; Moon, Y.; Pradhan, D.; Kim, S.-H.; Lee, H.-Y.; Lee, J. Experimental Investigation of Cavitation Bulk Nanobubbles Characteristics: Effects of pH and Surface-Active Agents. *Langmuir* **2023**, *39*, 1968−1986.
(34) Xu, Q.; Liang, L.; Nie, T.; She, Y.; Tao, L.; Guo, L. Effect of Electrolyte pH on Oxygen Bubble Behavior in Photoelectrochemical Water Splitting. *J. Phys. Chem. C* **2023**, *127*, 5308−5320.
(35) Lu, X.; Nie, T.; Li, X.; Jing, L.; Zhang, Y.; Ma, L.; Jing, D. Insight into pH-controlled Bubble Dynamics on a Pt Electrode During Electrochemical Water Splitting. *Phys. Fluids* **2023**, *35*, 103314.
(36) Xu, Q.; Tao, L.; Nie, T.; Liang, L.; She, Y.; Wang, M. Mechanism of pH Effect on Mass Transfer During Bubble Evolution on Photoelectrode Surfaces. *J. Electrochem. Soc.* **2024**, *171*, 016501.
(37) Fox, F. E.; Herzfeld, K. F. Gas Bubbles With Organic Skin as Cavitation Nuclei. *J. Acoust. Soc. Am.* **1954**, *26*, 984−989.
(38) Zhang, X.; Liu, X.; Zhong, Y.; Zhou, Z.; Huang, Y.; Sun, C. Q. Nanobubble Skin Supersolidity. *Langmuir* **2016**, *32*, 11321−11327.
(39) Yasui, K.; Tuziuti, T.; Kanematsu, W.; Kato, K. Dynamic Equilibrium Model for a Bulk Nanobubble and a Microbubble Partly Covered With Hydrophobic Material. *Langmuir* **2016**, *32*, 11101−11110.
(40) Azmin, M.; Mohamedi, G.; Edirisinghe, M.; Stride, E. Dissolution of Coated Microbubbles: The Effect of Nanoparticles and Surfactant Concentration. *Mater. Sci. Eng., C* **2012**, *32*, 2654−2658.
(41) Zhang, H.; Chen, S.; Guo, Z.; Zhang, X. The Fate of Bulk Nanobubbles Under Gas Dissolution. *Phys. Chem. Chem. Phys.* **2022**, *24*, 9685−9694.
(42) Ma, X.; Li, M.; Xu, X.; Sun, C. On the Role of Surface Charge and Surface Tension Tuned by Surfactant in Stabilizing Bulk Nanobubbles. *Appl. Surf. Sci.* **2023**, *608*, 155232.
(43) Bunkin, N. F.; Yurchenko, S. O.; Suyazov, N. V.; Shkirin, A. V. Structure of the Nanobubble Clusters of Dissolved Air in Liquid Media. *J. Biol. Phys.* **2012**, *38*, 121−152.
(44) Zhang, H.; Guo, Z.; Zhang, X. Surface Enrichment of Ions Leads to the Stability of Bulk Nanobubbles. *Soft Matter* **2020**, *16*, 5470−5477.
(45) Tan, B. H.; An, H.; Ohl, C.-D. How Bulk Nanobubbles Might Survive. *Phys. Rev. Lett.* **2020**, *124*, 134503.
(46) Satpute, P. A.; Earthman, J. C. Hydroxyl Ion Stabilization of Bulk Nanobubbles Resulting from Microbubble Shrinkage. *J. Colloid Interface Sci.* **2021**, *584*, 449−455.
(47) Li, M.; Ma, X.; Eisener, J.; Pfeiffer, P.; Ohl, C.-D.; Sun, C. How Bulk Nanobubbles Are Stable Over a Wide Range of Temperatures. *J. Colloid Interface Sci.* **2021**, *596*, 184−198.
(48) Ma, X.; Li, M.; Pfeiffer, P.; Eisener, J.; Ohl, C.-D.; Sun, C. Ion Adsorption Stabilizes Bulk Nanobubbles. *J. Colloid Interface Sci.* **2022**, *606*, 1380−1394.
(49) Ushikubo, F. Y.; Enari, M.; Furukawa, T.; Nakagawa, R.; Makino, Y.; Kawagoe, Y.; Oshita, S. Zeta-Potential of Micro-and/or Nano-Bubbles in Water Produced by Some Kinds of Gases. *IFAC Proc. Vol.* **2010**, *43*, 283−288.
(50) Oh, S. H.; Kim, J.-M. Generation and Stability of Bulk Nanobubbles. *Langmuir* **2017**, *33*, 3818−3823.
(51) Wang, X.; Li, P.; Ning, R.; Ratul, R.; Zhang, X.; Ma, J. Mechanisms on Stability of Bulk Nanobubble and Relevant Applications: A Review. *J. Cleaner Prod.* **2023**, *426*, 139153.

(52) Nirmalkar, N.; Pacek, A.; Barigou, M. Interpreting the Interfacial and Colloidal Stability of Bulk Nanobubbles. *Soft Matter* **2018**, *14*, 9643−9656.
(53) Ke, S.; Xiao, W.; Quan, N.; Dong, Y.; Zhang, L.; Hu, J. Formation and Stability of Bulk Nanobubbles in Different Solutions. *Langmuir* **2019**, *35*, 5250−5256.
(54) Kim, J.-Y.; Song, M.-G.; Kim, J.-D. Zeta Potential of Nanobubbles Generated by Ultrasonication in Aqueous Alkyl Polyglycoside Solutions. *J. Colloid Interface Sci.* **2000**, *223*, 285−291.
(55) Meegoda, J. N.; Aluthgun Hewage, S.; Batagoda, J. H. Stability of Nanobubbles. *Environ. Eng. Sci.* **2018**, *35*, 1216−1227.
(56) Li, Y.; Zhang, L.-W.; Wang, B. Role of Mutual Diffusion in the Dissolution Behavior of One Primary Bulk Gas Nanobubble in Liquid: A Molecular Dynamics Study. *Langmuir* **2023**, *39*, 7684−7693.
(57) Yen, T.-H.; Chen, Y.-L. Analysis of Gas Nanoclusters in Water Using All-Atom Molecular Dynamics. *Langmuir* **2022**, *38*, 13195−13205.
(58) Feng, M.; Ma, X.; Zhang, Z.; Luo, K. H.; Sun, C.; Xu, X. How Sodium Chloride Extends Lifetime of Bulk Nanobubbles in Water. *Soft Matter* **2022**, *18*, 2968−2978.
(59) Dixit, A. K.; Das, A. K. Molecular Approach for Understanding the Stability, Collision, and Coalescence of Bulk Nanobubbles. *Langmuir* **2022**, *38*, 16122−16133.
(60) Lu, Y.; Yang, L.; Kuang, Y.; Song, Y.; Zhao, J.; Sum, A. K. Molecular Simulations on the Stability and Dynamics of Bulk Nanobubbles in Aqueous Environments. *Phys. Chem. Chem. Phys.* **2021**, *23*, 27533−27542.
(61) Gao, Z.; Wu, W.; Sun, W.; Wang, B. Understanding the Stabilization of a Bulk Nanobubble: A Molecular Dynamics Analysis. *Langmuir* **2021**, *37*, 11281−11291.
(62) Hewage, S. A.; Meegoda, J. N. Molecular Dynamics Simulation of Bulk Nanobubbles. *Colloids Surf., A* **2022**, *650*, 129565.
(63) Zhang, P.; Feng, M.; Xu, X. Double-Layer Distribution of Hydronium and Hydroxide Ions in the Air−Water Interface. *ACS Phys. Chem. Au*, **2024**..
(64) Zhang, P.; Gardini, A. T.; Xu, X.; Parrinello, M. Intramolecular and Water Mediated Tautomerism of Solvated Glycine. *J. Chem. Inf. Model.* **2024**, *64*, 3599−3604.
(65) de Grotthuss, C. J. T. *Mémoire sur la Décomposition de l'Eau et des Corps qu'elle Tient en Dissolution à l'Aide de l'Électricité Galvanique*; University Of Wisconsin, 1805.
(66) Agmon, N. The Grotthuss Mechanism. *Chem. Phys. Lett.* **1995**, *244*, 456−462.
(67) Marx, D. Proton Transfer 200 Years After von Grotthuss: Insights from *Ab Initio* Simulations. *ChemPhysChem* **2006**, *7*, 1848−1870.
(68) Wang, H.; Zhang, L.; Han, J.; Weinan, E. DeePMD-kit: A Deep Learning Package for Many-Body Potential Energy Representation and Molecular Dynamics. *Comput. Phys. Commun.* **2018**, *228*, 178−184.
(69) Zeng, J.; Zhang, D.; Lu, D.; Mo, P.; Li, Z.; Chen, Y.; Rynik, M.; Huang, L.; Li, Z.; Shi, S.; et al. DeePMD-kit v2: A Software Package for Deep Potential Models. *J. Chem. Phys.* **2023**, *159*, 054801.
(70) Poli, E.; Jong, K. H.; Hassanali, A. Charge Transfer as a Ubiquitous Mechanism in Determining the Negative Charge at Hydrophobic Interfaces. *Nat. Commun.* **2020**, *11*, 901.
(71) Pullanchery, S.; Kulik, S.; Rehl, B.; Hassanali, A.; Roke, S. Charge Transfer Across C-H···O Hydrogen Bonds Stabilizes Oil Droplets in Water. *Science* **2021**, *374*, 1366−1370.
(72) Zhang, Y.; Wang, H.; Chen, W.; Zeng, J.; Zhang, L.; Wang, H.; Weinan, E. DP-GEN: A Concurrent Learning Platform for the Generation of Reliable Deep Learning Based Potential Energy Models. *Comput. Phys. Commun.* **2020**, *253*, 107206.
(73) Plimpton, S. Fast Parallel Algorithms for Short-Range Molecular Dynamics. *J. Comput. Phys.* **1995**, *117*, 1−19.
(74) Kresse, G.; Furthmüller, J. Efficient Iterative Schemes for *Ab Initio* Total-Energy Calculations Using a Plane-Wave Basis Set. *Phys. Rev. B* **1996**, *54*, 11169.
(75) Kresse, G.; Furthmüller, J. Efficiency of *Ab Initio* Total Energy Calculations for Metals and Semiconductors Using a Plane-Wave Basis Set. *Comput. Mater. Sci.* **1996**, *6*, 15−50.
(76) Sun, J.; Ruzsinszky, A.; Perdew, J. P. Strongly Constrained and Appropriately Normed Semilocal Density Functional. *Phys. Rev. Lett.* **2015**, *115*, 036402.
(77) Piaggi, P. M.; Weis, J.; Panagiotopoulos, A. Z.; Debenedetti, P. G.; Car, R. Homogeneous Ice Nucleation in an *Ab Initio* Machine-Learning Model of Water. *Proc. Natl. Acad. Sci. U. S. A.* **2022**, *119*, No. e2207294119.
(78) Zhang, L.; Wang, H.; Car, R.; Weinan, E. Phase Diagram of a Deep Potential Water Model. *Phys. Rev. Lett.* **2021**, *126*, 236001.
(79) Xu, J.; Zhang, C.; Zhang, L.; Chen, M.; Santra, B.; Wu, X. Isotope Effects in Molecular Structures and Electronic Properties of Liquid Water via Deep Potential Molecular Dynamics Based on the SCAN Functional. *Phys. Rev. B* **2020**, *102*, 214113.
(80) Liu, R.; Zhang, C.; Liang, X.; Liu, J.; Wu, X.; Chen, M. Structural and Dynamic Properties of Solvated Hydroxide and Hydronium Ions in Water from *Ab Initio* Modeling. *J. Chem. Phys.* **2022**, *157*, 024503.
(81) Zheng, L.; Chen, M.; Sun, Z.; Ko, H.-Y.; Santra, B.; Dhuvad, P.; Wu, X. Structural, Electronic, and Dynamical Properties of Liquid Water by *Ab Initio* Molecular Dynamics Based on SCAN Functional Within the Canonical Ensemble. *J. Chem. Phys.* **2018**, *148*, 164505.
(82) Chen, M.; Ko, H.-Y.; Remsing, R. C.; Andrade, M. F. C.; Santra, B.; Sun, Z.; Selloni, A.; Car, R.; Klein, M. L.; Perdew, J. P.; Wu, X. *Ab Initio* Theory and Modeling of Water. *Proc. Natl. Acad. Sci. U. S. A.* **2017**, *114*, 10846−10851.
(83) Methfessel, M.; Paxton, A. High-Precision Sampling for Brillouin-Zone Integration in Metals. *Phys. Rev. B* **1989**, *40*, 3616.
(84) Gartner III, T. E.; Zhang, L.; Piaggi, P. M.; Car, R.; Panagiotopoulos, A. Z.; Debenedetti, P. G. Signatures of a Liquid−Liquid Transition in an *Ab Initio* Deep Neural Network Model for Water. *Proc. Natl. Acad. Sci. U. S. A.* **2020**, *117*, 26040−26046.
(85) Sanchez-Burgos, I.; Muniz, M. C.; Espinosa, J. R.; Panagiotopoulos, A. Z. A Deep Potential Model for Liquid−Vapor Equilibrium and Cavitation Rates of Water. *J. Chem. Phys.* **2023**, *158*, 184504.
(86) Calegari Andrade, M.; Car, R.; Selloni, A. Probing the Self-Ionization of Liquid Water With *Ab Initio* Deep Potential Molecular Dynamics. *Proc. Natl. Acad. Sci. U. S. A.* **2023**, *120*, No. e2302468120.
(87) Gillan, M. J.; Alfe, D.; Michaelides, A. Perspective: How Good Is DFT for Water? *J. Chem. Phys.* **2016**, *144*, 130901.
(88) Nosé, S. A Unified Formulation of the Constant Temperature Molecular Dynamics Methods. *J. Chem. Phys.* **1984**, *81*, 511−519.
(89) Hoover, W. G. Canonical Dynamics: Equilibrium Phase-Space Distributions. *Phys. Rev. A* **1985**, *31*, 1695.
(90) Martins-Costa, M. T.; Ruiz-López, M. F. Electrostatics and Chemical Reactivity at the Air−Water Interface. *J. Am. Chem. Soc.* **2023**, *145*, 1400−1406.
(91) Miguel de la Puente, M.; David, R.; Gomez, A.; Laage, D. Acids at the Edge: Why Nitric and Formic Acid Dissociations at Air−Water Interfaces Depend on Depth and on Interface Specific Area. *J. Am. Chem. Soc.* **2022**, *144*, 10524−10529.
(92) Zhang, P.; Xu, X. Propensity of Water Self-Ions at Air (Oil)-Water Interfaces Revealed by Deep Potential Molecular Dynamics With Enhanced Sampling. *arXiv* **2024**, .
(93) Mamatkulov, S. I.; Allolio, C.; Netz, R. R.; Bonthuis, D. J. Orientation-Induced Adsorption of Hydrated Protons at the Air−Water Interface. *Angew. Chem., Int. Ed.* **2017**, *56*, 15846−15851.
(94) Liu, J.; Yang, J.; Zeng, X. C.; Xantheas, S. S.; Yagi, K.; He, X. Towards Complete Assignment of the Infrared Spectrum of the Protonated Water Cluster $H^+(H_2O)_{21}$. *Nat. Commun.* **2021**, *12*, 6141.
(95) Ahmed, A. K. A.; Sun, C.; Hua, L.; Zhang, Z.; Zhang, Y.; Marhaba, T.; Zhang, W. Colloidal Properties of Air, Oxygen, and Nitrogen Nanobubbles in Water: Effects of Ionic Strength, Natural Organic Matters, and Surfactants. *Environ. Eng. Sci.* **2018**, *35*, 720−727.

(96) Boshenyatov, B.; Kosharidze, S.; Levin, Y. K. On the Stability of Nanobubbles in Water. *Russ. Phys. J.* **2019**, *61*, 1914−1921.
(97) Yasui, K.; Tuziuti, T.; Kanematsu, W. Mysteries of Bulk Nanobubbles (Ultrafine Bubbles); Stability and Radical Formation. *Ultrason. Sonochem.* **2018**, *48*, 259−266.
(98) Gor, G. Y.; Kuchma, A. E. Dynamics of Gas Bubble Growth in a Supersaturated Solution With Sievert's Solubility Law. *J. Chem. Phys.* **2009**, *131*, 034507.
(99) Van Der Waals, J. D.; Rowlinson, J. S. *On the Continuity of the Gaseous and Liquid States*; Courier Corporation, 2004.
(100) Cassone, G. Nuclear Quantum Effects Largely Influence Molecular Dissociation and Proton Transfer in Liquid Water Under an Electric Field. *J. Phys. Chem. Lett.* **2020**, *11*, 8983−8988.
(101) Sviridov, A. P.; Osminkina, L. A.; Nikolaev, A. L.; Kudryavtsev, A. A.; Vasiliev, A. N.; Timoshenko, V. Y. Lowering of the Cavitation Threshold in Aqueous Suspensions of Porous Silicon Nanoparticles for Sonodynamic Therapy Applications. *Appl. Phys. Lett.* **2015**, *107*, 123107.
(102) Oliveira, H.; Azevedo, A.; Rubio, J. Nanobubbles Generation in a High-Rate Hydrodynamic Cavitation Tube. *Miner. Eng.* **2018**, *116*, 32−34.
(103) Etchepare, R.; Oliveira, H.; Nicknig, M.; Azevedo, A.; Rubio, J. Nanobubbles: Generation Using a Multiphase Pump, Properties and Features in Flotation. *Miner. Eng.* **2017**, *112*, 19−26.
(104) Xu, W.; Lu, Z.; Sun, X.; Jiang, L.; Duan, X. Superwetting Electrodes for Gas-Involving Electrocatalysis. *Acc. Chem. Res.* **2018**, *51*, 1590−1598.
(105) Zhao, X.; Ren, H.; Luo, L. Gas Bubbles in Electrochemical Gas Evolution Reactions. *Langmuir* **2019**, *35*, 5392−5408.
(106) Lee, J. K.; Walker, K. L.; Han, H. S.; Kang, J.; Prinz, F. B.; Waymouth, R. M.; Nam, H. G.; Zare, R. N. Spontaneous Generation of Hydrogen Peroxide from Aqueous Microdroplets. *Proc. Natl. Acad. Sci. U. S. A.* **2019**, *116*, 19294−19298.
(107) Jiang, H.; Sun, Y.; You, B. Dynamic Electrodeposition on Bubbles: An Effective Strategy Toward Porous Electrocatalysts for Green Hydrogen Cycling. *Acc. Chem. Res.* **2023**, *56*, 1421−1432.
(108) Jin, S.; Chen, H.; Yuan, X.; Xing, D.; Wang, R.; Zhao, L.; Zhang, D.; Gong, C.; Zhu, C.; Gao, X.; Chen, Y.; Zhang, X. The Spontaneous Electron-Mediated Redox Processes on Sprayed Water Microdroplets. *JACS Au* **2023**, *3*, 1563−1571.
(109) Das, S.; Imoto, S.; Sun, S.; Nagata, Y.; Backus, E. H.; Bonn, M. Nature of Excess Hydrated Proton at the Water−Air Interface. *J. Am. Chem. Soc.* **2020**, *142*, 945−952.
(110) Litman, Y.; Chiang, K.-Y.; Seki, T.; Nagata, Y.; Bonn, M. Surface Stratification Determines the Interfacial Water Structure of Simple Electrolyte Solutions. *Nat. Chem.* **2024**, *16*, 644−650.


https://doi.org/10.1021/jacs.4c06641
*J. Am. Chem. Soc.* 2024, 146, 19537−19546